Metal-insulator transition and quantum magnetism in the SU(3) Fermi-Hubbard model

Chunhan Feng [1], Eduardo Ibarra-García-Padilla [2,3], Kaden R. A. Hazzard [4,5,3], Richard Scalettar [3], Shiwei Zhang [1], and Ettore Vitali [6]

[1] *Center for Computational Quantum Physics, Flatiron Institute, 162 5th Avenue, New York, New York 10010, USA*
[2] *Department of Physics and Astronomy, San José State University, San José, California 95192, USA*
[3] *Department of Physics and Astronomy, University of California, Davis, California 95616, USA*
[4] *Department of Physics and Astronomy, Rice University, Houston, Texas 77005, USA*
[5] *Rice Center for Quantum Materials, Rice University, Houston, Texas 77005, USA*
[6] *Department of Physics, California State University Fresno, Fresno, California 93720, USA*

(Received 7 July 2023; revised 17 October 2023; accepted 22 November 2023; published 20 December 2023)

We develop a self-consistent variant of the constrained path quantum Monte Carlo approach which ensures its independence of the trial wave function, and apply the method to compute ground-state correlations in the two-dimensional SU(3) Fermi-Hubbard Hamiltonian at $\frac{1}{3}$ filling, modeling fermions with three possible spin flavors moving on a square lattice with an average of one particle per site. We provide clear evidence of a quantum critical point separating a nonmagnetic uniform metallic phase from a regime where long-range "spin" order is present. This discovery of multiple successive transitions to magnetic states with regular, long-range alternation of the different flavors, whose symmetry changes as the interaction strength increases, significantly extends previous work in the Heisenberg limit to itinerant fermions. In addition to the rich quantum magnetism, this important physical system allows one to study integer filling and the associated Mott transition disentangled from nesting, in contrast to the usual SU(2) model, while preserving the square-lattice geometry. Our results also provide a significant step towards the interpretation of present and future experiments on fermionic alkaline-earth atoms, and other realizations of SU(N) physics.

DOI: 10.1103/PhysRevResearch.5.043267

I. INTRODUCTION

The Fermi-Hubbard model (FHM) [1,2] is a paradigmatic description of strongly correlated materials [3,4]. In its original single-band, SU(2)-symmetric form, it exhibits a wealth of physics including a metal-to-insulator transition at half-filling [5], as well as ferromagnetic and antiferromagnetic orders across its interaction-filling phase diagram [6–9]. On a square lattice, upon doping away from half-filling, it also manifests more subtle physics including strange metallicity, a pseudogap, spin-charge "stripe" domains, and d-wave pairing, phenomena central to the cuprate superconductors [10–12].

However, in this geometry and at half-filling the properties of the SU(2) Hubbard Hamiltonian are determined simultaneously by the special features of the noninteracting dispersion, perfect nesting at $k = (\pi, \pi)$, and by the onsite repulsion U. This leads to the anomalous feature that the critical interaction strength for the metal-insulator transition is $U_c = 0$, and a blurring of "Slater" insulating behavior associated with the opening of an antiferromagnetic gap at (π, π), and the Mott insulator which does not rely on long-range magnetic symmetry breaking but only on the high-energy cost for local double occupancy. While such a separation is also possible by invoking a triangular or kagome geometry, our work does so while preserving the bipartite square lattice whose study is central to many experiments.

The SU(N) Hubbard model, which features larger spins and an enhanced symmetry, has been intensively studied [13–23], in part because quantum fluctuations are expected to give rise to a more complex set of low-temperature spin structures. A rich phenomenology has been predicted in the ground state in the Heisenberg limit ($U \gg t$ at $\langle n \rangle = 1$) [24–33], including an antiferromagnetic (AFM) ground state with a three-sublattice pattern at the wave vector $k = (\pm 2\pi/3, \pm 2\pi/3)$ [25,32]. The physics away from this limit has been less explored, with existing results largely focused on fairly high-temperature properties, employing methods that are uncontrolled at low temperature [13,15,16,34–39], or restricted to one dimension [40–43], or on different geometries [44], or half-filling for even N [45–49] (which is challenging to reach due to particle losses in experiments with ultracold atoms in optical lattices).

Driven by interest in cuprate superconductivity, auxiliary-field quantum Monte Carlo (AFQMC) approaches initially focused on single-orbital, square-lattice geometries with two spin species. However, as new materials and phases came to the forefront, AFQMC played a key role in their study, Dirac fermions and semimetal phases on a honeycomb lattice being one prominent example [50,51]. The rapid development of experiments with ultracold alkaline-earth-like atoms (AEAs)

that exhibit a natural SU(N)-symmetric interaction [52–62] provides a concrete and exciting setting to explore the intriguing phases noted above, and offers a similar opportunity for AFQMC to play a major role in an emerging area of strongly correlated quantum matter. Ongoing experiments aiming to pair quantum gas microscopes [63–66] with AEAs are expected to soon enable real-space imaging of correlations, which demands a deeper understanding of the order in the SU(N) Hubbard model.

It is a major challenge to obtain reliable answers to the question we address here, namely, the ground-state properties of the SU(3) FHM on a two-dimensional (2D) square lattice at $\frac{1}{3}$ filling. A high-accuracy treatment is required in a strongly correlated system, as well as large supercell sizes to extract the thermodynamic limit. Unlike its SU(2) counterpart, a fermion sign problem [67] is present in the SU(3) model at $\langle n\rangle = 1$. In this paper we use an implementation of the constrained path (CP) auxiliary-field quantum Monte Carlo (AFQMC) methodology [68] which iteratively refines the constraining Slater determinant [69] to solve this important problem of strong current experimental interest. This allows us to quantify the location of the QCP and determine a phase diagram. Above a critical interaction strength U_c which is roughly half the bandwidth, the system develops AFM order. We also discover two previously unknown intermediate orders (which we label 3-2 and 3-4 AFM) along the route to the large-U Heisenberg limit.

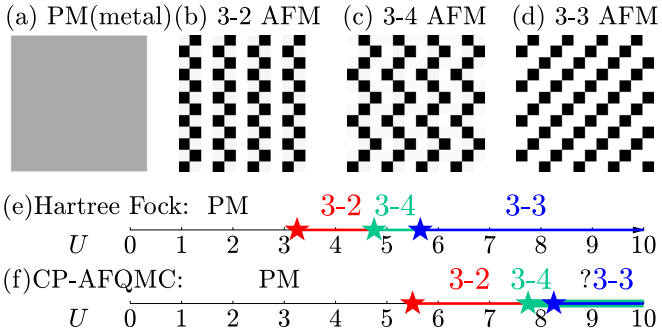

FIG. 1. Phase diagram of the $\frac{1}{3}$-filling SU(3) Fermi-Hubbard Model. [(a)–(d)] Schematic density correlations for one of the three spin species in different phases on a $N = 12 \times 12$ square lattice. (a) At small $U < U_{c1}$, the system resides in a paramagnetic (PM) phase, as indicated by the uniform gray color map. (b) For $U_{c1} < U < U_{c2}$ a nonuniform pattern emerges which has period 3 in one direction and 2 in the other, which we denote by "3-2 AFM" phase. (c) $U_{c2} < U < U_{c3}$ is similarly denoted as "3-4 AFM" and (d) finally, for $U > U_{c3}$, the order is a "3-3 AFM." (e) Hartree-Fock phase diagram: The quantum phase transition points are $U_{c1}^{\mathrm{MF}} \approx 3.25$, $U_{c2}^{\mathrm{MF}} \approx 4.75$, and $U_{c3}^{\mathrm{MF}} \approx 5.65$. (f) AFQMC phase diagram: $U_{c1} \approx 5.5$, $U_{c2} \approx 7.7$, and $U_{c3} \approx 8.3$. The question mark indicates that, although 3-3 has a slightly lower energy, it cannot be clearly distinguished from 3-4 in our calculations.

II. HAMILTONIAN AND METHODOLOGY

The SU(3) FHM is defined by the Hamiltonian

$$H = -t \sum_{\langle i,j\rangle,\sigma} (c_{i\sigma}^{\dagger} c_{j\sigma} + \mathrm{H.c.}) + \frac{U}{2} \sum_{i,\sigma\neq\tau} n_{i\sigma} n_{i\tau}, \qquad (1)$$

where $c_{i\sigma}^{\dagger}$ ($c_{i\sigma}$) is the creation (annihilation) operator for a fermion with spin flavor $\sigma = A, B, C$ on site i on a 2D square lattice. $N_s = L_x \times L_y$ denotes the number of lattice sites, $n_{i\sigma} = c_{i\sigma}^{\dagger} c_{i\sigma}$ is the number operator for flavor σ on site i, $\langle i, j\rangle$ denotes nearest-neighbor pairs, t is the hopping amplitude which will serve as the energy unit, and U is the interaction strength. We study the ground state of the Hamiltonian in Eq. (1) as a function of U in the spin-balanced case at $\frac{1}{3}$ filling (where there is an average of one fermion per lattice site), that is, in the sector of Hilbert space with $N_A = N_B = N_C = N_s/3$. To characterize the ground-state properties, we measure energies, correlation functions, and structure factors. For example, the spin-resolved two-body correlation functions $\langle n_i^{\sigma} n_j^{\tau}\rangle \equiv \langle \phi_0 | n_i^{\sigma} n_j^{\tau} | \phi_0 \rangle$. This is complemented by the corresponding momentum-space measures, for example, the equal time, equal species, density structure factor $S(k) = \frac{1}{3}\sum_{\sigma} S_{\sigma\sigma}(k) = \frac{1}{3N_s}\sum_{i,j,\sigma}\langle (n_i^{\sigma} - \langle n_i^{\sigma}\rangle)(n_j^{\sigma} - \langle n_j^{\sigma}\rangle)\rangle e^{ik(r_i - r_j)}$, where r_i and r_j are the coordinates of sites i and j.

We perform unrestricted Hartree-Fock (UHF) calculations as preliminary explorations to suggest candidate phases of matter, and to generate trial wave functions for AFQMC (see below). In the UHF treatment we approximate the Hamiltonian as $H_{\mathrm{HF}} = \sum_{\sigma} H_{\mathrm{HF}}^{\sigma}$, where $H_{\mathrm{HF}}^{\sigma} = -t\sum_{\langle i,j\rangle}(c_{i\sigma}^{\dagger} c_{j\sigma} + \mathrm{H.c.}) + U_{\mathrm{eff}}\sum_{i,\tau\neq\sigma}(\langle n_{i\tau}\rangle n_{i\sigma} - \frac{1}{2}\langle n_{i\tau}\rangle\langle n_{i\sigma}\rangle)$, and determine the mean fields $\langle n_{i\sigma}\rangle$ self-consistently from values initialized randomly or constructed from several possible ordered patterns proposed for the $\frac{1}{3}$-filling SU(3) FHM [15,16]. Our method reproduces the SU(2) UHF phase diagram [6,70]. In H_{HF}^{σ} above we have allowed an effective interaction strength U_{eff}, which does not have to equal the "physical" U. This turns out to be important in verifying the independence of final results on the trial wave function (Hartree-Fock solution) with different U_{eff} (see Appendix). As discussed in more detail later, the four phases depicted in Fig. 1 emerge as mean-field ground states for different values of the interaction strength; however, estimates of the critical values of U could differ significantly from the exact result.

In order to compute the ground-state properties beyond the mean-field level, we use the state-of-the-art CP-AFQMC method [68,71]. AFQMC is a projection quantum Monte Carlo approach, based on the fact that the ground state can be obtained by acting an imaginary-time-evolution operator on a trial wave function, $|\phi_0\rangle \propto \lim_{\tau\to\infty} e^{-\tau H}|\phi_T\rangle$, as long as the trial wave function is nonorthogonal to the ground state $\langle\phi_T|\phi_0\rangle \neq 0$. Within AFQMC, a combination of the Trotter decomposition and the Hubbard-Stratonovich transformation maps the imaginary-time evolution onto a random walk in the manifold of Slater determinants, and ground-state properties are averages over this random walk. Observables are measured by back-propagation [68,72] in the open-ended random walk approach of CP-AFQMC.

AFQMC yields exact ground-state correlations in special situations, like the SU($2N$) Hubbard model at half-filling [36,41,46], and electron-phonon Hamiltonians including the Holstein [73–78] and the Su-Schrieffer-Heeger models [79–83]. In the SU(3) model, the infamous fermion sign problem [67,84–86] necessitates a constrained path approximation which imposes a sign or gauge condition on the sampling in

auxiliary-field space [68,87] relying on a trial wave function. In this work we leverage the recent methodological advances [69] to implement self-consistency loops which minimize the biases related to the trial wave function. The very promising success of such techniques in the SU(2) model, in both the repulsive [88–91] and attractive regimes [92], together with several cross-checks we did in this work (Appendix, Fig. 5, and analysis below), demonstrates the high accuracy of the method.

III. RESULTS

Our main results are summarized in Fig. 1, as a ground-state phase diagram of the $\frac{1}{3}$-filling ($\langle n\rangle = 1$) SU(3) FHM. Figures 1(a)–1(d) illustrate the patterns in the magnetic correlations in each of the phases. Black and white represent high- and low-density correlations for a single flavor, respectively. The many-body phase diagram is given in Fig. 1(f). [The UHF result is shown in Fig. 1(e) for reference and comparison.] At small U, the system is in a paramagnetic (PM) (metal) phase, while at large U, multiple occupancies are suppressed and superexchange causes adjacent sites to favor different spin species, and therefore generates an antiferromagnetic (AFM) pattern. In contrast to the SU(2) case where the AFM correlation determines a unique (up to translations) spatial pattern, many patterns are possible for SU(3). We find multiple ordering vectors occur, representing distinct ground states for different U values. Figure 1(b) has a period of 3 in one direction and 2 in the other direction, thus it is denoted as a 3-2 AFM. Similarly, patterns 1(c) and 1(d) are denoted 3-4 and 3-3 AFM, respectively.

Within the Hartree-Fock treatment, we have $U_{c1}^{\mathrm{MF}} \sim 3.25$ below which the system is in the paramagnetic phase. When $3.25 \lesssim U \lesssim 4.75$, the 3-2 AFM has a lower energy with respect to the other two states, while the 3-4 AFM is the ground state for the intermediate region $4.75 \lesssim U \lesssim 5.65$. However, the energy gap to other orders in this intermediate regime is relatively small. The 3-3 AFM is the mean-field ground state for the large-U region $U \gtrsim 5.65$. The corresponding phase diagram from AFQMC is shown in Fig. 1(f). As expected, the metal-insulator phase transition happens at a larger $U_{c1} \sim 5.5 > U_{c1}^{\mathrm{MF}} \sim 3.25$ than in UHF, reflecting the fact that the latter overestimates the ordering tendency due to its absence of fluctuations. As in UHF, AFQMC also gives the 3-3 AFM as the ground state at large U, consistent with the ground state found in prior work in the Heisenberg limit [25]. However, the energy of this state, obtained from AFQMC, is nearly degenerate with the 3-4 pattern for the larger-U values investigated here.

The three AFM phases can be characterized by spin-resolved two-body correlations $\langle n_i^\sigma n_j^\tau\rangle$. The correlations are displayed in Fig. 2 along the real-space path $r_i - r_j = (0,0) \to (6,0) \to (6,6)$ in a 12×12 square lattice. Figures 2(a), 2(c), and 2(e) are for $U = 7, 8, 9$, and correspond to the 3-2, 3-4, and 3-3 AFM phases, respectively. Different spin-flavor correlations are depicted by different colors. Along the x direction, as seen from separations (0,0) to (6,0), the correlations in all three AFM phases alternate "ABCABC..." (period 3), while in the y directions, 3-2, 3-4, and 3-3 AFM have periods 2, 4, 3, respectively. The single-flavor structure

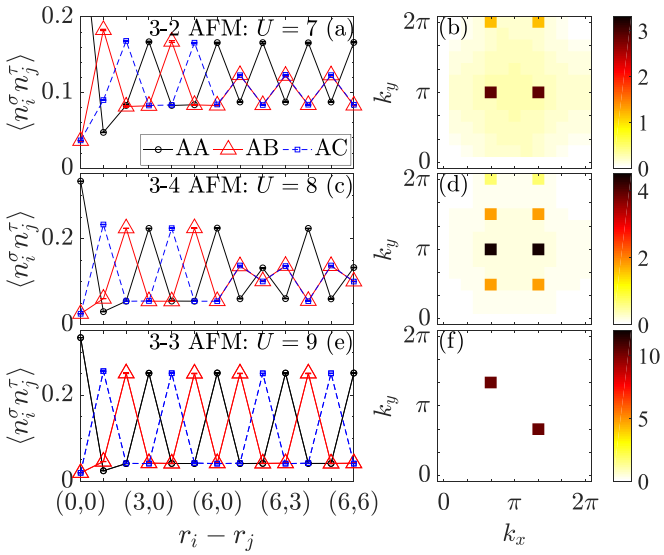

FIG. 2. (a), (c), (e) Spin-resolved two-body correlations $\langle n_i^\sigma n_j^\tau\rangle$ as a function of $r_i - r_j$, the vector connecting site i and j, at $U = 7$ (3-2 AFM), $U = 8$ (3-4 AFM), $U = 9$ (3-3 AFM) given by AFQMC on a 12×12 lattice. Different colors represent different spin species $\{\sigma, \tau\} = AA; AB; AC$. (b), (d), (f) The single-flavor structure factor $S_{\sigma\sigma}(k)$ as a function of momenta $k = (k_x, k_y)$ for the systems in (a), (c), and (e), respectively.

factor $S_{\sigma\sigma}(k)$, which is a Fourier transform of the corresponding real-space two-body correlations, is plotted as a function of k in Figs. 2(b), 2(d), and 2(f). The 3-2, 3-4, and 3-3 AFM phases have peaks at distinct k points, appropriate to the periodicity of the real-space patterns of Figs. 1(b)–1(d).

To further characterize the phase in different U regions, the ground-state structure factor at the three characteristic momenta $k = (2\pi/3, \pi/2), (2\pi/3, \pi), (2\pi/3, 4\pi/3)$ are shown in Fig. 3 as functions of U. The vertical lines separate the

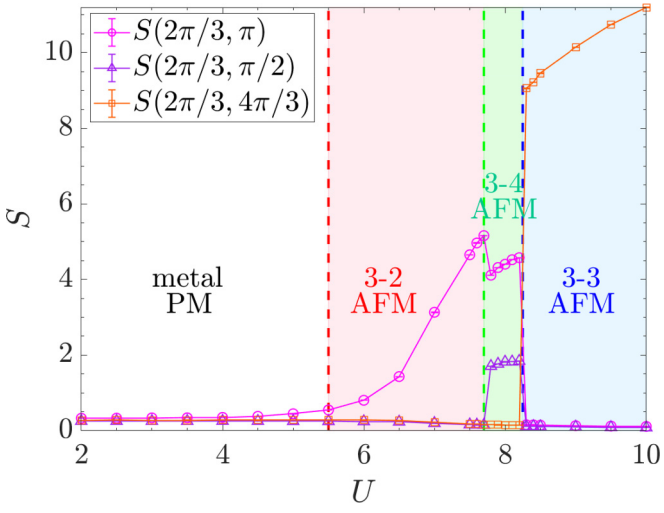

FIG. 3. The structure factor $S(k)$ at characteristic $k = (k_x, k_y)$ values of $(2\pi/3, \pi/2)$, $(2\pi/3, \pi)$, $(2\pi/3, 4\pi/3)$ as a function of U on a 12×12 lattice. The AFQMC calculations are started with several different possible trial ground states for each U. The one with the lowest energy after convergence of the self-consistent iteration is shown here.

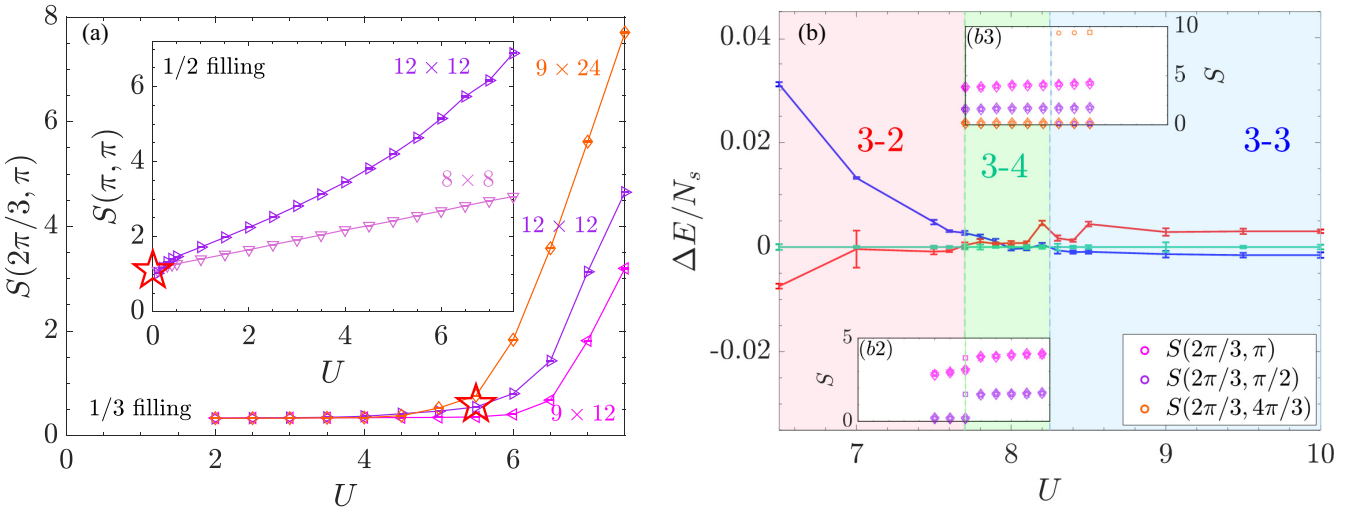

FIG. 4. Determining the transition points between phases. (a) The 3-2 AFM structure factor vs U is shown for three lattice sizes. $S(2\pi/3,\pi)$ is small and nearly independent of the system size in the metallic phase but grows proportionally to system size in the 3-2 AFM phase. The boundary between the two regimes gives the metal-insulator phase transition point U_{c1}. The inset shows $S(\pi,\pi)$ for $\frac{1}{2}$ filling, which exhibits a critical point at $U=0$, in contrast with the finite U_{c1} at $\frac{1}{3}$ filling. (b) Energy differences with respect to the 3-4 AFM phase. Red, green, and blue curves represent 3-2, 3-4, and 3-3 AFM states, respectively. Insets (b2) and (b3) show complementary results on structure factors to help validate the location of U_{c2} and U_{c3}. In each, the calculations use a trial wave function constructed from the superposition of the two states involved, and the two corresponding structure factors are shown. Different symbol shapes represent results from different random seeds.

regimes where the different AFM orders are stable. There is no peak in the PM metal; in the 3-2 phase, a peak is present at $k=(2\pi/3,\pi)$; in the 3-4 phase, peaks are seen at both $k=(2\pi/3,\pi)$ and $(2\pi/3,\pi/2)$; finally, the 3-3 AFM phase shows a peak at $k=(2\pi/3,4\pi/3)$. In a UHF calculation, the phase boundary can be determined by either searching for the global ground state at each U, or by comparing the energies of different self-consistent ordered solutions, ensuring in either cases that the thermodynamic limit is reached. This is challenging to execute in many-body computations where statistical error bars and (much larger) finite-size effects can exceed energy differences. We use a combination of strategies to resolve the different boundaries as illustrated in Fig. 4.

The transition between the PM metal and the 3-2 AFM phases can be observed with robust and unambiguous self-consistent AFQMC calculations. In Fig. 4(a), we show the computed structure factor $S(2\pi/3,\pi)$ as a function of U for a number of lattice sizes. At each U, we start the calculation from a trial wave function generated from UHF with an essentially arbitrary $U_{\rm eff}$, and perform self-consistency via the natural orbitals [69]. The self-consistent iteration consistently converges to the same final value (see Fig. 5 in the Appendix) which is shown in the plot. The existence of the QCP U_{c1} is evident from the different size dependencies of $S(2\pi/3,\pi)$ as U is varied across it. Extrapolating the finite-temperature compressibilities leads to a U_{c1} [93] consistent with our results. A sharp contrast is seen between this behavior and that at $\frac{1}{2}$ filling, shown in the inset of Fig. 4(a), emphasizing the result of decoupling of nesting from the Mott transition: At $\langle n\rangle=\frac{3}{2}$, the spins form an alternating pattern "A(B&C)A(B&C)..." which singles out one species (e.g., A) with the other two (B and C) behaving interchangeably [13]. This spin arrangement has period 2 in both the x and y directions, hence giving rise to a structure factor peak at (π,π). In this case, the dependence of the structure factor on lattice size starts as soon as the interaction U is turned on, implying that the long-range order develops at $U_{c1}=0$, similar to the half-filling case in the SU(2) Hubbard model. This is expected since the SU(3) case also has the same perfectly nested Fermi surface at $k=(\pi,\pi)$, as argued in [13].

To determine the nature of the ordered AFM phases, we apply complementary measurements, with additional non-self-consistent calculations using multideterminant trial wave functions. As discussed above, the UHF solutions using different $U_{\rm eff}$ can produce distinct patterns, which can be used as trial wave function and the initial Slater determinant to start our AFQMC calculations at any U. However, this turns the whole procedure from a linear process (projection) into a nonlinear process, which can get stuck in local minima. In this situation, we determine the true ground state by comparing the energies obtained from different constraints, as illustrated in Fig. 4(b). Three regions are seen, with the lowest energies given by the 3-2, 3-4, and 3-3 states, respectively. Their boundaries, where two energy curves cross, give two more transition points, U_{c2} and U_{c3}. AFQMC with single Slater determinant constraints typically achieves energy accuracy of well over subpercent level [87–89,91]. When the energy difference becomes much smaller, we augment our process: in the vicinity of U_{c2} we use a superposition of two Slater determinants corresponding to 3-2 and 3-4 AFM as the trial wave function. This leads to a finite structure factor $S(2\pi/3,\pi)$ (3-2 AFM order) on one side, in contrast with finite $S(2\pi/3,\pi)$ and $S(2\pi/3,\pi/2)$ (3-4) on the other, as illustrated in Fig. 4(b2). Near $U\sim U_{c3}$, we conduct the same

procedures, as shown in Fig. 4(b3). Beyond $U/t \sim 8.25$, however, even this procedure leads to ambiguous results, where both 3-4 and 3-3 structure factors can become finite, depending on the random number seed. This combined with the tiny energy differences indicates that, to within the resolution of the current calculations, the 3-4 and 3-3 orders are essentially degenerate for the larger-U values investigated here.

IV. DISCUSSION

Using a high-accuracy many-body numerical computation, we have mapped out the ground-state phase diagram of the two-dimensional SU(3) Hubbard model at $\frac{1}{3}$ filling (one particle per site). We find a metal-insulator phase transition at the QCP $U_{c1} \sim 5.5$, above which long-range magnetic orders develop. Compared to the more ubiquitous SU(2) counterpart, the SU(3) case allows the separation of strong interaction effects at integer filling from nongeneric features of band structure: nesting of the Fermi surface and a van Hove singularity in the density of states. An immediate consequence is the nonzero value of U_c.

Above U_{c1}, our results suggest two intermediate magnetic orders (3-2 and 3-4 AFM phases) before the final, strong coupling 3-3 phase. We determined the critical interaction strengths for the ordering wave vectors by comparing their energies and also by using a superposition of two states as the initial and trial wave functions in our AFQMC calculations. The results given by these two approaches are consistent. Beyond $U_{c3} \sim 8.25$, the 3-3 AFM energy appears to be slightly lower than 3-4 AFM, but they are almost degenerate at the interaction strengths considered in the study.

The metal-insulator transitions and magnetic ordered phases predicted in our work provide important steps to understand SU(N) physics. This is especially timely with the intense experimental efforts to emulate such systems using ultracold AEAs. How these magnetic orders evolve at finite temperature and other potentially exotic phases in the doped systems emerge are interesting questions for future work, especially in the experimental context.

ACKNOWLEDGMENTS

We thank Zewen Zhang for the discovery of the 3-4 order within Hartree-Fock calculations as well as useful discussions. E.V. acknowledges support from the National Science Foundation Award No. 2207048. Several calculations have been performed using the ACCESS-XSEDE allocation. R.T.S. and E.I.-G.-P. are supported by the Grant No. DE-SC-0022311, funded by the U.S. Department of Energy, Office of Science. K.R.A.H and E.I.-G.-P. acknowledge support from the Robert A. Welch Foundation (Grant No. C-1872), the National Science Foundation (Grant No. PHY-1848304), and the W. F. Keck Foundation (Grant No. 995764). Computing resources were supported in part by the Big-Data Private-Cloud Research Cyberinfrastructure MRI-award funded by NSF under Grant No. CNS-1338099 and by Rice University's Center for Research Computing (CRC). K.H.'s contribution benefited from discussions at the Aspen Center for Physics, supported by the National Science Foundation Grant No. PHY-1066293, and the KITP, which was supported in part by the National Science Foundation under Grant No. NSF PHY-1748958. We thank the Flatiron Institute Scientific Computing Center for computational resources. The Flatiron Institute is a division of the Simons Foundation.

APPENDIX

In this Appendix, we present additional details concerning (1) self-consistency procedures we conduct in the constrained path auxiliary-field quantum Monte Carlo (CP-AFQMC) method; (2) comparisons of energies in different phases and finite lattice size effect analysis in the Hartree-Fock.

1. Self-consistency: Real-space spin correlations

In this paper we have implemented a self-consistent CP-AFQMC approach, described in [69]. An example of the convergence of the same-spin density-density correlations $\langle n_i^A n_j^A \rangle$ is given in Fig. 5 to illustrate this process. The calculation is initiated from a Slater determinant given by the $U_{\text{eff}} = 3.5$ Hartree-Fock 3-2 AFM solution and the one-body density matrix is obtained from QMC. We diagonalize the one-body density matrix and find the eigenvectors which correspond to the largest N_σ eigenvalues. Those eigenvectors are used to construct a new Slater determinant, which is then

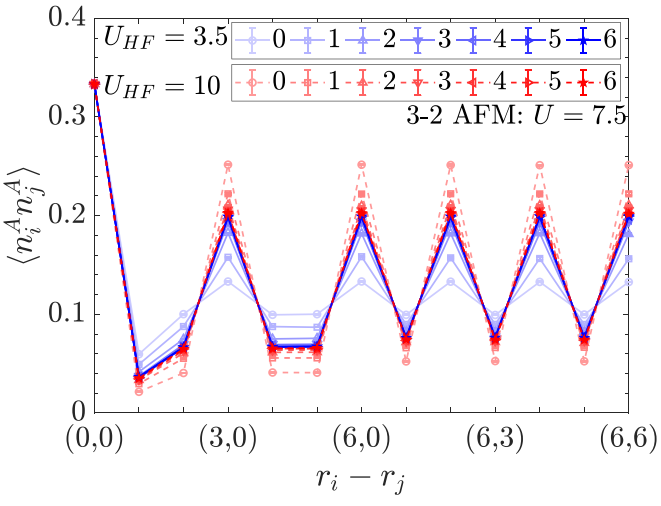

FIG. 5. Illustration of convergence of real-space density-density correlation. We have chosen $U_{c1} < U = 7.5 < U_{c2}$, where the system is in the 3-2 AF phase. Spin correlations converge from lower and higher values when the starting point is in the 3-2 phase using an initial Slater determinant with $U_{\text{eff}} = 3.5$ and 10, respectively. The legend indicates the number of self-consistent iterations.

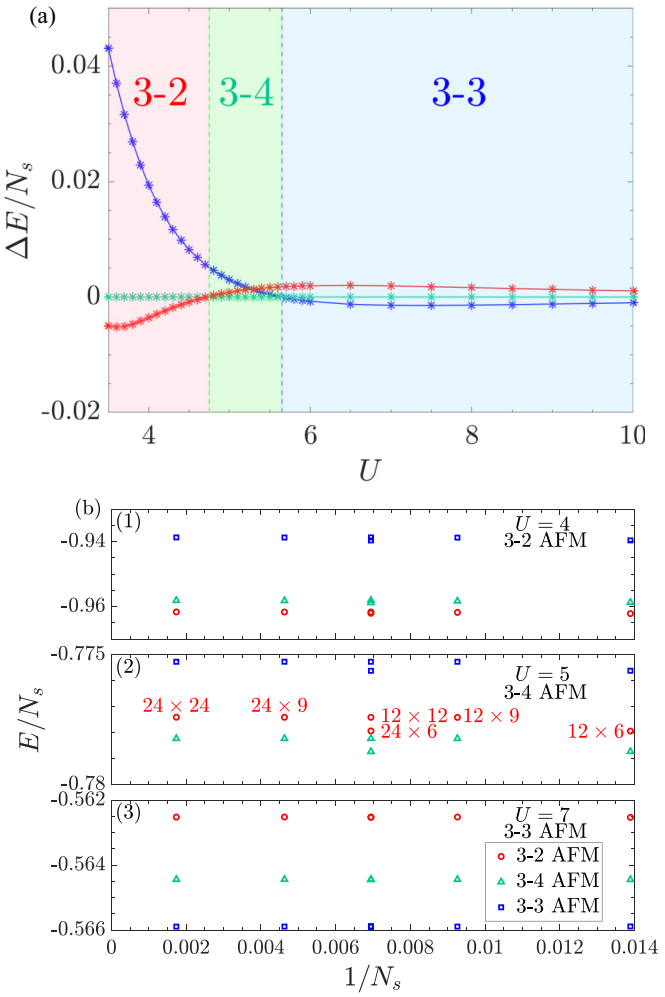

FIG. 6. (a) The energy difference $\Delta E = E - E_{\text{3-4 AFM}}$ (3-4 AFM energy is viewed as a reference) per site given by Hartree-Fock as a function of interaction strength. 3-2, 3-4, 3-3 AFM energies are depicted by red, green, and blue curves respectively. (b) Energy per site E/N_s vs $1/N_s$, given by the Hartree-Fock calculation for $U = 4, 5, 7$, corresponding to "3-2," "3-4," and "3-3" AFM phases, respectively. The lattice sizes $L_x \times L_y$ are labeled next to the data points in panel (2) as examples. Different symbols in the legend represent the possible "local minimum" orders.

used as the initial Slater determinant for the next iteration of simulation. The number in the legend of Fig. 5 indicates the self-consistent iteration value. Blue right triangles ("5" in the legend) and blue stars ("6") are almost on top of each other, implying the density-density correlations converge after ∼6 self-consistent iterations.

As a check that the results are independent of initialization, we also start our simulation with another initial Slater determinant, obtained from the $U_{\text{eff}} = 10$, 3-2 AFM Hartree-Fock solution. The results (red stars) agree with the one starting from the $U_{\text{eff}} = 3.5$ Hartree-Fock (blue star). All results presented in the main text are given by the last self-consistent (fully converged) iteration.

2. Finite lattice size effects: Energy

In Fig. 6, we explore finite lattice size effects in the Hartree-Fock calculations. First, similar to Fig. 4(b), we show the total energy difference per site $\Delta E/N_s$ given by Hartree-Fock as a function of U for a 12×12 square lattice in Fig. 6(a). The 3-2, 3-4, and 3-3 AFM phase has the lowest energy for $U_{c1}^{\text{MF}} \lesssim U \lesssim U_{c2}^{\text{MF}}$, $U_{c2}^{\text{MF}} \lesssim U \lesssim U_{c3}^{\text{MF}}$, and $U \gtrsim U_{c3}^{\text{MF}}$, respectively. In order to detect whether the small energy difference at strong interactions is due to the finite lattice size effect, we choose $U = 4$ (3-2 phase), $U = 5$ (3-4 phase), and $U = 7$ (3-3 phase) and present the energy per site E/N_s as a function of $1/N_s$ in Fig. 6(b). Different symbols in the legend represent the local minimum 3-2, 3-4, 3-3 AFM states. Lattice sizes are labeled next to the data points in Fig. 6(b)(2). We can extrapolate the energy to the thermodynamic limit $1/N_s \to 0$. There is no crossing between different AFM phases, implying the energy ordering between the three magnetic phases on the 12×12 lattice in Fig. 6(a) still holds in the thermodynamic limit. We have also verified that this conclusion is robust to the application twisted boundary conditions to the lattice and taking the average of energies for different twist angles. This method effectively samples a finer mesh of momentum points and hence larger spatial sizes [94–96].

[1] J. Hubbard, Electron correlations in narrow energy bands, Proc. R. Soc. London A **276**, 238 (1963).

[2] M. C. Gutzwiller, Correlation of electrons in a narrow s band, Phys. Rev. **137**, A1726 (1965).

[3] M. Rasetti, *The Hubbard Model: Recent Results* (World Scientific, Singapore, 1991), Vol. 7.

[4] D. Scalapino, Distinguishing high-T_c theories, J. Phys. Chem. Solids **56**, 1669 (1995).

[5] F. Gebhard, *Metal-insulator Transitions* (Springer, Berlin, 1997).

[6] J. E. Hirsch, Two-dimensional Hubbard model: Numerical simulation study, Phys. Rev. B **31**, 4403 (1985).

[7] S. R. White, D. J. Scalapino, R. L. Sugar, E. Y. Loh, J. E. Gubernatis, and R. T. Scalettar, Numerical study of the two-dimensional Hubbard model, Phys. Rev. B **40**, 506 (1989).

[8] P. Fazekas, *Lecture Notes on Electron Correlation and Magnetism* (World Scientific, Singapore, 1999), Vol. 5.

[9] H. Xu, H. Shi, E. Vitali, M. Qin, and S. Zhang, Stripes and spin-density waves in the doped two-dimensional Hubbard model: Ground state phase diagram, Phys. Rev. Res. **4**, 013239 (2022).

[10] H. Tasaki, The Hubbard model - an introduction and selected rigorous results, J. Phys.: Condens. Matter **10**, 4353 (1998).

[11] D. P. Arovas, E. Berg, S. A. Kivelson, and S. Raghu, The Hubbard model, Annu. Rev. Condens. Matter Phys. **13**, 239 (2022).

[12] M. Qin, T. Schäfer, S. Andergassen, P. Corboz, and E. Gull, The Hubbard model: A computational perspective, Annu. Rev. Condens. Matter Phys. **13**, 275 (2022).

[13] C. Honerkamp and W. Hofstetter, Ultracold fermions and the SU(N) Hubbard model, Phys. Rev. Lett. **92**, 170403 (2004).

[14] I. Titvinidze, A. Privitera, S.-Y. Chang, S. Diehl, M. A. Baranov, A. Daley, and W. Hofstetter, Magnetism and domain formation in SU(3)-symmetric multi-species Fermi mixtures, New J. Phys. **13**, 035013 (2011).

[15] A. Sotnikov and W. Hofstetter, Magnetic ordering of three-component ultracold fermionic mixtures in optical lattices, Phys. Rev. A **89**, 063601 (2014).

[16] A. Sotnikov, Critical entropies and magnetic-phase-diagram analysis of ultracold three-component fermionic mixtures in optical lattices, Phys. Rev. A **92**, 023633 (2015).

[17] M. Hafez-Torbati and W. Hofstetter, Artificial SU(3) spin-orbit coupling and exotic Mott insulators, Phys. Rev. B **98**, 245131 (2018).

[18] M. Hafez-Torbati and W. Hofstetter, Competing charge and magnetic order in fermionic multicomponent systems, Phys. Rev. B **100**, 035133 (2019).

[19] M. Hafez-Torbati, J.-H. Zheng, B. Irsigler, and W. Hofstetter, Interaction-driven topological phase transitions in fermionic SU(3) systems, Phys. Rev. B **101**, 245159 (2020).

[20] W. Nie, D. Zhang, and W. Zhang, Ferromagnetic ground state of the SU(3) Hubbard model on the Lieb lattice, Phys. Rev. A **96**, 053616 (2017).

[21] E. V. Gorelik and N. Blümer, Mott transitions in ternary flavor mixtures of ultracold fermions on optical lattices, Phys. Rev. A **80**, 051602(R) (2009).

[22] A. Pérez-Romero, R. Franco, and J. Silva-Valencia, Phase diagram of the SU(3) Fermi Hubbard model with next-neighbor interactions, Eur. Phys. J. B **94**, 229 (2021).

[23] E. Ibarra-García-Padilla, S. Dasgupta, H.-T. Wei, S. Taie, Y. Takahashi, R. T. Scalettar, and K. R. A. Hazzard, Universal thermodynamics of an SU(N) Fermi-Hubbard model, Phys. Rev. A **104**, 043316 (2021).

[24] M. Hermele, V. Gurarie, and A. M. Rey, Mott insulators of ultracold fermionic alkaline earth atoms: Underconstrained magnetism and chiral spin liquid, Phys. Rev. Lett. **103**, 135301 (2009).

[25] T. A. Tóth, A. M. Läuchli, F. Mila, and K. Penc, Three-sublattice ordering of the SU(3) Heisenberg model of three-flavor fermions on the square and cubic lattices, Phys. Rev. Lett. **105**, 265301 (2010).

[26] M. Hermele and V. Gurarie, Topological liquids and valence cluster states in two-dimensional SU(N) magnets, Phys. Rev. B **84**, 174441 (2011).

[27] P. Nataf and F. Mila, Exact diagonalization of Heisenberg SU(N) models, Phys. Rev. Lett. **113**, 127204 (2014).

[28] P. Corboz, A. M. Läuchli, K. Penc, M. Troyer, and F. Mila, Simultaneous dimerization and SU(4) symmetry breaking of 4-color fermions on the square lattice, Phys. Rev. Lett. **107**, 215301 (2011).

[29] B. Bauer, P. Corboz, A. M. Läuchli, L. Messio, K. Penc, M. Troyer, and F. Mila, Three-sublattice order in the SU(3) Heisenberg model on the square and triangular lattice, Phys. Rev. B **85**, 125116 (2012).

[30] D. Yamamoto, C. Suzuki, G. Marmorini, S. Okazaki, and N. Furukawa, Quantum and thermal phase transitions of the triangular SU(3) Heisenberg model under magnetic fields, Phys. Rev. Lett. **125**, 057204 (2020).

[31] P. Nataf, M. Lajkó, P. Corboz, A. M. Läuchli, K. Penc, and F. Mila, Plaquette order in the SU(6) Heisenberg model on the honeycomb lattice, Phys. Rev. B **93**, 201113(R) (2016).

[32] C. Romen and A. M. Läuchli, Structure of spin correlations in high-temperature SU(N) quantum magnets, Phys. Rev. Res. **2**, 043009 (2020).

[33] H. Song and M. Hermele, Mott insulators of ultracold fermionic alkaline earth atoms in three dimensions, Phys. Rev. B **87**, 144423 (2013).

[34] K. R. A. Hazzard, V. Gurarie, M. Hermele, and A. M. Rey, High-temperature properties of fermionic alkaline-earth-metal atoms in optical lattices, Phys. Rev. A **85**, 041604(R) (2012).

[35] L. Bonnes, K. R. A. Hazzard, S. R. Manmana, A. M. Rey, and S. Wessel, Adiabatic loading of one-dimensional SU(N) alkaline-earth-atom fermions in optical lattices, Phys. Rev. Lett. **109**, 205305 (2012).

[36] Z. Cai, H.-H. Hung, L. Wang, D. Zheng, and C. Wu, Pomeranchuk cooling of SU($2N$) ultracold fermions in optical lattices, Phys. Rev. Lett. **110**, 220401 (2013).

[37] A. Cichy and A. Sotnikov, Orbital magnetism of ultracold fermionic gases in a lattice: Dynamical mean-field approach, Phys. Rev. A **93**, 053624 (2016).

[38] A. Golubeva, A. Sotnikov, A. Cichy, J. Kuneš, and W. Hofstetter, Breaking of SU(4) symmetry and interplay between strongly correlated phases in the Hubbard model, Phys. Rev. B **95**, 125108 (2017).

[39] V. Unukovych and A. Sotnikov, SU(4)-symmetric Hubbard model at quarter filling: Insights from the dynamical mean-field approach, Phys. Rev. B **104**, 245106 (2021).

[40] S. R. Manmana, K. R. A. Hazzard, G. Chen, A. E. Feiguin, and A. M. Rey, SU(N) magnetism in chains of ultracold alkaline-earth-metal atoms: Mott transitions and quantum correlations, Phys. Rev. A **84**, 043601 (2011).

[41] S. Xu, J. T. Barreiro, Y. Wang, and C. Wu, Interaction effects with varying N in SU(N) symmetric fermion lattice systems, Phys. Rev. Lett. **121**, 167205 (2018).

[42] R. Assaraf, P. Azaria, M. Caffarel, and P. Lecheminant, Metal-insulator transition in the one-dimensional SU(N) Hubbard model, Phys. Rev. B **60**, 2299 (1999).

[43] S. Capponi, P. Lecheminant, and K. Totsuka, Phases of one-dimensional SU(N) cold atomic Fermi gases—From molecular Luttinger liquids to topological phases, Ann. Phys. **367**, 50 (2016).

[44] S. S. Chung and P. Corboz, SU(3) fermions on the honeycomb lattice at $\frac{1}{3}$ filling, Phys. Rev. B **100**, 035134 (2019).

[45] N. Blümer and E. V. Gorelik, Mott transitions in the half-filled SU($2M$) symmetric Hubbard model, Phys. Rev. B **87**, 085115 (2013).

[46] D. Wang, L. Wang, and C. Wu, Slater and Mott insulating states in the SU(6) Hubbard model, Phys. Rev. B **100**, 115155 (2019).

[47] D. Wang, Y. Li, Z. Cai, Z. Zhou, Y. Wang, and C. Wu, Competing orders in the 2D half-filled SU($2N$) Hubbard model through the pinning-field quantum Monte Carlo simulations, Phys. Rev. Lett. **112**, 156403 (2014).

[48] Z. Cai, H.-H. Hung, L. Wang, and C. Wu, Quantum magnetic properties of the $SU(2N)$ Hubbard model in the square lattice: A quantum Monte Carlo study, Phys. Rev. B **88**, 125108 (2013).

[49] F. F. Assaad, Phase diagram of the half-filled two-dimensional SU(N) Hubbard-Heisenberg model: A quantum Monte Carlo study, Phys. Rev. B **71**, 075103 (2005).

[50] Z. Meng, T. Lang, S. Wessel, F. Assaad, and A. Muramatsu, Quantum spin liquid emerging in two-dimensional correlated Dirac fermions, Nature (London) **464**, 847 (2010).

[51] Y. Otsuka, S. Yunoki, and S. Sorella, Universal quantum criticality in the metal-insulator transition of two-dimensional interacting dirac electrons, Phys. Rev. X **6**, 011029 (2016).

[52] A. V. Gorshkov, M. Hermele, C. Xu, P. S. Julienne, J. Ye, P. Zoller, E. Demler, M. D. Lukin, and A. M. Rey, Two-orbital SU(N) magnetism with ultracold alkaline-earth atoms, Nat. Phys. **6**, 289 (2010).

[53] M. A. Cazalilla and A. M. Rey, Ultracold Fermi gases with emergent SU(N) symmetry, Rep. Prog. Phys. **77**, 124401 (2014).

[54] C. Wu, J.-P. Hu, and S.-C. Zhang, Exact SO(5) symmetry in the spin-3/2 fermionic system, Phys. Rev. Lett. **91**, 186402 (2003).

[55] M. A. Cazalilla, A. F. Ho, and M. Ueda, Ultracold gases of ytterbium: ferromagnetism and Mott states in an SU(6) Fermi system, New J. Phys. **11**, 103033 (2009).

[56] S. Taie, R. Yamazaki, S. Sugawa, and Y. Takahashi, An SU(6) Mott insulator of an atomic Fermi gas realized by large-spin Pomeranchuk cooling, Nat. Phys. **8**, 825 (2012).

[57] C. Hofrichter, L. Riegger, F. Scazza, M. Höfer, D. R. Fernandes, I. Bloch, and S. Fölling, Direct probing of the Mott crossover in the SU(N) Fermi-Hubbard model, Phys. Rev. X **6**, 021030 (2016).

[58] H. Ozawa, S. Taie, Y. Takasu, and Y. Takahashi, Antiferromagnetic spin correlation of SU($\mathcal{N}$) Fermi gas in an optical superlattice, Phys. Rev. Lett. **121**, 225303 (2018).

[59] S. Taie, E. Ibarra-García-Padilla, N. Nishizawa, Y. Takasu, Y. Kuno, H.-T. Wei, R. T. Scalettar, K. R. A. Hazzard, and Y. Takahashi, Observation of antiferromagnetic correlations in an ultracold SU(N) Hubbard model, Nat. Phys. **18**, 1356 (2022).

[60] Y. Takahashi, Quantum simulation of quantum many-body systems with ultracold two-electron atoms in an optical lattice, Proc. Jpn. Acad., Ser. B **98**, 141 (2022).

[61] D. Tusi, L. Franchi, L. F. Livi, K. Baumann, D. Benedicto Orenes, L. Del Re, R. E. Barfknecht, T.-W. Zhou, M. Inguscio, G. Cappellini, M. Capone, J. Catani, and L. Fallani, Flavour-selective localization in interacting lattice fermions, Nat. Phys. **18**, 1201 (2022).

[62] G. Pasqualetti, O. Bettermann, N. D. Oppong, E. Ibarra-García-Padilla, S. Dasgupta, R. T. Scalettar, K. R. A. Hazzard, I. Bloch, and S. Fölling, Equation of state and thermometry of the 2D SU(N) Fermi-Hubbard model, arXiv:2305.18967.

[63] C. Gross and I. Bloch, Quantum simulations with ultracold atoms in optical lattices, Science **357**, 995 (2017).

[64] I. Bloch, J. Dalibard, and S. Nascimbène, Quantum simulations with ultracold quantum gases, Nat. Phys. **8**, 267 (2012).

[65] R. Yamamoto, J. Kobayashi, T. Kuno, K. Kato, and Y. Takahashi, An ytterbium quantum gas microscope with narrow-line laser cooling, New J. Phys. **18**, 023016 (2016).

[66] C. Gross and W. S. Bakr, Quantum gas microscopy for single atom and spin detection, Nat. Phys. **17**, 1316 (2021).

[67] E. Y. Loh, Jr., J. E. Gubernatis, R. T. Scalettar, S. R. White, D. J. Scalapino, and R. L. Sugar, Sign problem in the numerical simulation of many-electron systems, Phys. Rev. B **41**, 9301 (1990).

[68] S. Zhang, J. Carlson, and J. E. Gubernatis, Constrained path Monte Carlo method for fermion ground states, Phys. Rev. B **55**, 7464 (1997).

[69] M. Qin, H. Shi, and S. Zhang, Coupling quantum Monte Carlo and independent-particle calculations: Self-consistent constraint for the sign problem based on the density or the density matrix, Phys. Rev. B **94**, 235119 (2016).

[70] J. Xu, C.-C. Chang, E. J. Walter, and S. Zhang, Spin- and charge-density waves in the Hartree–Fock ground state of the two-dimensional Hubbard model, J. Phys.: Condens. Matter **23**, 505601 (2011).

[71] H. Shi and S. Zhang, Symmetry in auxiliary-field quantum Monte Carlo calculations, Phys. Rev. B **88**, 125132 (2013).

[72] W. Purwanto and S. Zhang, Quantum Monte Carlo method for the ground state of many-boson systems, Phys. Rev. E **70**, 056702 (2004).

[73] M. Hohenadler and G. G. Batrouni, Dominant charge density wave correlations in the Holstein model on the half-filled square lattice, Phys. Rev. B **100**, 165114 (2019).

[74] C. Feng and R. T. Scalettar, Interplay of flat electronic bands with Holstein phonons, Phys. Rev. B **102**, 235152 (2020).

[75] C. Feng, H. Guo, and R. T. Scalettar, Charge density waves on a half-filled decorated honeycomb lattice, Phys. Rev. B **101**, 205103 (2020).

[76] C. Chen, X. Y. Xu, Z. Y. Meng, and M. Hohenadler, Charge-density-wave transitions of Dirac fermions coupled to phonons, Phys. Rev. Lett. **122**, 077601 (2019).

[77] Y. Zhang, C. Feng, R. Mondaini, G. G. Batrouni, and R. T. Scalettar, Charge singlets and orbital-selective charge density wave transitions, Phys. Rev. B **106**, 115120 (2022).

[78] C. Kvande, C. Feng, F. Hébert, G. G. Batrouni, and R. T. Scalettar, Enhancement of charge density wave correlations in a holstein model with an anharmonic phonon potential, Phys. Rev. B **108**, 075119 (2023).

[79] C. Feng, B. Xing, D. Poletti, R. Scalettar, and G. Batrouni, Phase diagram of the Su-Schrieffer-Heeger-Hubbard model on a square lattice, Phys. Rev. B **106**, L081114 (2022).

[80] X. Cai, Z.-X. Li, and H. Yao, Antiferromagnetism induced by bond Su-Schrieffer-Heeger electron-phonon coupling: A quantum Monte Carlo study, Phys. Rev. Lett. **127**, 247203 (2021).

[81] B. Xing, W.-T. Chiu, D. Poletti, R. T. Scalettar, and G. Batrouni, Quantum Monte Carlo simulations of the 2D Su-Schrieffer-Heeger model, Phys. Rev. Lett. **126**, 017601 (2021).

[82] A. Götz, S. Beyl, M. Hohenadler, and F. F. Assaad, Valence-bond solid to antiferromagnet transition in the two-dimensional Su-Schrieffer-Heeger model by Langevin dynamics, Phys. Rev. B **105**, 085151 (2022).

[83] B. Xing, C. Feng, R. Scalettar, G. G. Batrouni, and D. Poletti, Attractive Su-Schrieffer-Heeger-Hubbard model on a square lattice away from half-filling, Phys. Rev. B **108**, L161103 (2023).

[84] M. Troyer and U.-J. Wiese, Computational complexity and fundamental limitations to fermionic quantum Monte Carlo simulations, Phys. Rev. Lett. **94**, 170201 (2005).

[85] C. J. Umrigar, J. Toulouse, C. Filippi, S. Sorella, and R. G. Hennig, Alleviation of the fermion-sign problem by optimization of many-body wave functions, Phys. Rev. Lett. **98**, 110201 (2007).

[86] R. Mondaini, S. Tarat, and R. T. Scalettar, Quantum critical points and the sign problem, Science **375**, 418 (2022).

[87] C.-C. Chang and S. Zhang, Spatially inhomogeneous phase in the two-dimensional repulsive Hubbard model, Phys. Rev. B **78**, 165101 (2008).

[88] J. P. F. LeBlanc, A. E. Antipov, F. Becca, I. W. Bulik, G. K.-L. Chan, C.-M. Chung, Y. Deng, M. Ferrero, T. M. Henderson, C. A. Jiménez-Hoyos, E. Kozik, X.-W. Liu, A. J. Millis, N. V. Prokof'ev, M. Qin, G. E. Scuseria, H. Shi, B. V. Svistunov, L. F. Tocchio, I. S. Tupitsyn *et al.* (Simons Collaboration on the Many-Electron Problem), Solutions of the two-dimensional Hubbard model: Benchmarks and results from a wide range of numerical algorithms, Phys. Rev. X **5**, 041041 (2015).

[89] B.-X. Zheng, C.-M. Chung, P. Corboz, G. Ehlers, M.-P. Qin, R. M. Noack, H. Shi, S. R. White, S. Zhang, and G. K.-L. Chan, Stripe order in the underdoped region of the two-dimensional Hubbard model, Science **358**, 1155 (2017).

[90] M. Qin, C.-M. Chung, H. Shi, E. Vitali, C. Hubig, U. Schollwöck, S. R. White, and S. Zhang (Simons Collaboration on the Many-Electron Problem), Absence of superconductivity in the pure two-dimensional Hubbard model, Phys. Rev. X **10**, 031016 (2020).

[91] M. Qin, H. Shi, and S. Zhang, Benchmark study of the two-dimensional Hubbard model with auxiliary-field quantum Monte Carlo method, Phys. Rev. B **94**, 085103 (2016).

[92] E. Vitali, P. Rosenberg, and S. Zhang, Exotic superfluid phases in spin-polarized Fermi gases in optical lattices, Phys. Rev. Lett. **128**, 203201 (2022).

[93] E. Ibarra-García-Padilla, C. Feng, G. Pasqualetti, S. Fölling, R. T. Scalettar, E. Khatami, and K. R. A. Hazzard, Metal-insulator transition and magnetism of SU(3) fermions in the square lattice Phys. Rev. A **108**, 053312 (2023).

[94] S. Sorella, Finite-size scaling with modified boundary conditions, Phys. Rev. B **91**, 241116(R) (2015).

[95] C. Gros, Control of the finite-size corrections in exact diagonalization studies, Phys. Rev. B **53**, 6865 (1996).

[96] C. Lin, F. H. Zong, and D. M. Ceperley, Twist-averaged boundary conditions in continuum quantum Monte Carlo algorithms, Phys. Rev. E **64**, 016702 (2001).